Laminar-Turbulent Transition Research in the Boeing/AFOSR Mach-6 Quiet Tunnel

AIAA Paper 2005-0888, Presented at the 43rd Fluid Dynamics Conference, Reno, NV, Jan. 2005

Steven P. Schneider[*], Craig Skoch[†], Shann Rufer[‡], Erick Swanson[§], and Matthew P. Borg[¶]
School of Aeronautics and Astronautics
Purdue University
West Lafayette, IN 47907-1282

Abstract

Laminar-turbulent transition is critical for vehicles which fly at hypersonic speeds for extended periods. To improve on existing correlations, prediction methods that incorporate knowledge of the transition mechanisms are necessary and now feasible. Purdue continues to develop the Boeing/AFOSR Mach-6 Tunnel to seek quiet flow at high Reynolds number, with noise levels comparable to flight. The loss of quiet flow above 8 psia stagnation pressure is probably not due to fluctuations exiting the driver tube, since preliminary measurements show these are comparable to those in the Langley Mach 3.5 quiet tunnel. Studies of the effect of downstream disturbances show that separation is more likely for a laminar nozzle-wall boundary layer, as expected; there is still no evidence that such disturbances can trip the upstream boundary layer. An eighth bleed-slot insert was designed and tested, but was not useful, since the suction massflow was too large to maintain a sonic throat. A porthole window has been completed for high Reynolds number operation to 6×10^6/ft., which should enable temperature-sensitive paints measurements of blunt-cone transition induced by surface roughness. Finally, preliminary hot-wire measurements appear to show second-mode instability waves on a blunt cone at 235 kHz.

[*]Professor. Associate Fellow, AIAA.
[†]Research Assistant. Student Member, AIAA.
[‡]Research Assistant. Student Member, AIAA.
[§]Research Assistant. Student Member, AIAA.
[¶]Research Assistant. Student Member, AIAA.

Introduction

Hypersonic Laminar-Turbulent Transition

Laminar-turbulent transition in hypersonic boundary layers is important for prediction and control of heat transfer, skin friction, and other boundary layer properties. Vehicles that spend extended periods at hypersonic speeds may be critically affected by the uncertainties in transition prediction, depending on their Reynolds numbers. However, the mechanisms leading to transition are still poorly understood, even in low-noise environments.

Many transition experiments have been carried out in conventional ground-testing facilities over the past 50 years [1]. However, these experiments are contaminated by the high levels of noise that radiate from the turbulent boundary layers normally present on the wind tunnel walls [2]. These noise levels, typically 0.5-1% of the mean, are an order of magnitude larger than those observed in flight [3, 4]. These high noise levels can cause transition to occur an order of magnitude earlier than in flight [2, 4]. In addition, the mechanisms of transition operational in small-disturbance environments can be changed or bypassed altogether in high-noise environments; these changes in the mechanisms change the parametric trends in transition [3]. Mechanism-based prediction methods must be developed, supported in part with measurements of the mechanisms in quiet wind tunnels.

Development of Quiet-Flow Wind Tunnels

Only in the last two decades have low-noise supersonic wind tunnels been developed [2, 5]. This development has been difficult, since the test-section wall boundary-layers must be kept laminar in order to avoid high levels of eddy-Mach-wave acoustic radiation

from the normally-present turbulent boundary layers. A Mach 3.5 tunnel was the first to be successfully developed at NASA Langley [6]. Langley then developed a Mach 6 quiet nozzle, which was used as a starting point for the new Purdue nozzle [7]. Unfortunately, this nozzle was removed from service due to a space conflict; it is now to be reinstalled at Texas A&M. The Purdue Mach-6 tunnel is presently the only operational hypersonic tunnel with any quiet flow, anywhere in the world.

Background of the Boeing/AFOSR Mach-6 Quiet Tunnel

A Mach-4 Ludwieg tube was developed at Purdue in 1992-1994 [8]. Quiet flow was achieved at low Reynolds numbers, and the facility was used for development of instrumentation and for measurements of instability waves under quiet-flow conditions. However, the low quiet Reynolds number and the small 4-inch test section imposed severe limitations.

A low-cost hypersonic facility that remains quiet to higher Reynolds numbers is needed. Beginning with Ref. [9], a series of AIAA papers have reported on the design, fabrication, and shakedown of this facility, on the development of instrumentation, and on progress towards achieving Mach-6 quiet flow at high Reynolds number.

Ref. [10] summarized these earlier papers, reported on initial quiet flow achieved at low Reynolds numbers with the 6th bleed-slot design, and also on initial measurements with temperature-sensitive paints and hot wires. Ref. [11] reported temperature-sensitive-paints results on the forebody, the results of the 7th bleed-slot throat geometry, and the (minimal) effect of polishing the downstream portion of the Mach-6 nozzle. Ref. [12] reported initial measurements of bypass transition on the nozzle wall, the reduction of low-pressure separation after removing the double-wedge model-support centerbody, and high levels of static-pressure fluctuations in the diffuser when the nozzle-wall boundary layer is laminar, as well as hot-wire and temperature-paints measurements on a sharp cone. Ref. [13] reported more measurements of bypass transition on the nozzle wall, along with the disappointingly minor effect of bypassing the bleed-slot air direct to the vacuum tanks. It also reports more measurements in the diffuser, the first measurements in the contraction entrance, initial measurements of condensation, the successful fabrication of a new sting support, and preliminary hot-wire measurements on cones, along with hot-wire calibrations. Ref. [14] reported uncalibrated measurements of the fluctuations in the contraction entrance, the negligible effect of introducing small controlled disturbances in the driver tube, the helium-sniffer leak tests, initial work towards high-pressure operation, and the effect of downstream disturbances from small jets. It also reported temperature effects on the Kulite calibrations, and progress with the hot-wire calibrations and stability measurements.

The present paper reports progress in the second half of 2004. Efforts to achieve quiet flow at high Reynolds number presently fall into three categories: 1) measurements in the contraction entrance, seeking noise sources in the flow entering the throat, 2) measurements downstream of the nozzle, seeking evidence regarding the possible upstream propagation of downstream noise sources, and 3) computations of the flow in the bleed slot, seeking evidence of fluctuations that can trip the flow downstream. Recent computations show that a separation bubble is forming on the main-flow side of the bleed lip [15]; at present, this appears to be the most likely cause of early transition. However, the other approaches continue to be studied in parallel. In addition, the tunnel and instrumentation continue to be developed for study of the transition mechanisms and for conventional-noise operation at high unit Reynolds number.

The Boeing/AFOSR Mach-6 Quiet Tunnel

Quiet facilities require low levels of noise in the inviscid flow entering the nozzle through the throat, and laminar boundary layers on the nozzle walls. To reach these low noise levels, conventional blow-down facilities must be extensively modified. Requirements include a 1 micron particle filter, a highly polished nozzle with bleed slots for the contraction-wall boundary layer, and a large settling chamber with screens and sintered-mesh plates for noise-reduction [2]. To reach these low noise levels in an affordable way, the Purdue facility has been designed as a Ludwieg tube [8]. A Ludwieg tube is a long pipe with a converging-diverging nozzle on the end, from which flow exits into the nozzle, test section, and second throat (Figure 1). A diaphragm is placed downstream of the test section. When the diaphragm bursts, an expansion wave travels upstream through the test section into the driver tube. Since the flow remains quiet after the wave reflects from the contraction, sufficient vacuum can extend the useful runtime to many cycles of expansion-wave reflection, during which the pressure drops quasi-statically.

Two methods are now available to provide flow in the nozzle-throat bleed slots. A fast valve remains connected directly between the bleeds and the vacuum tank, allowing the bleed air to be dumped directly into the tank, with a small but significant delay of about 1/2 sec., which increases to perhaps 2 sec. at very

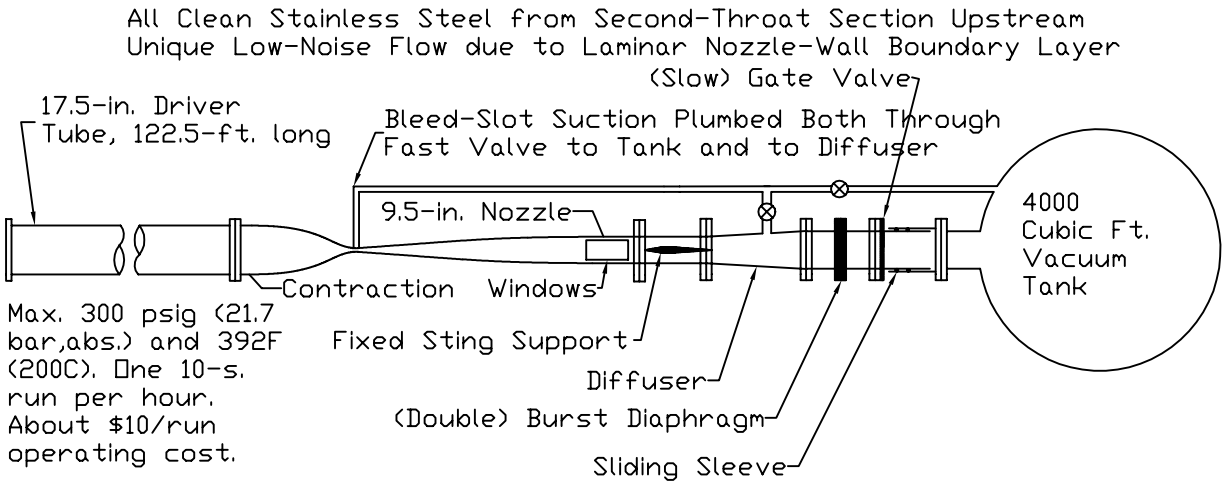

Figure 1: Schematic of Boeing/AFOSR Mach-6 Quiet Tunnel

low pressures, where the existing valve does not work well. In addition, the original plumbing connecting the bleed air to the diffuser has been reconnected. A tee permits the use of either valve. This fast valve to the tank has the advantage of eliminating any difficulties associated with the jets of air in the diffuser, but delays the startup of the flow, and does not open well at very low pressures. The ball valves to the diffuser allow quick passive timing of the start up, but introduce jets of air into the diffuser. Since recent measurements suggest that these jets are usually not a problem, this simple passive timing is again desirable.

Figure 2 shows the nozzle. Here, z is an axial coordinate whose origin is at the nozzle throat. The region of useful quiet flow lies between the characteristics marking the onset of uniform flow, and the characteristics marking the upstream boundary of acoustic radiation from the onset of turbulence in the nozzle-wall boundary layer. A 7.5-deg. sharp cone is drawn on the figure. The rectangles are drawn on the nozzle at the location of window openings, all but one of which are presently filled with blank metal inserts. Images of the tunnel are available at `http://roger.ecn.purdue.edu/~aae519/BAM6QT-Mach-6-tunnel/`, along with earlier papers and other documentation.

Pre-Run Free Convection in the Contraction Entrance

One of the sources of early transition on the nozzle walls could be fluctuations in the flow entering the nozzle throat. Although considerable care was taken to obtain clean, dry, stagnant air of uniform temperature in the driver tube and contraction, nonuniformities may still exist. To investigate this possibility, it is desirable to make measurements in the driver tube and contraction. This is not easy, since both are ASME code-stamped pressure vessels, and not readily modified. However, measurements are possible using two access ports provided at the entrance to the contraction, near the driver tube exit. The access ports are centered 6.500 inches downstream of the beginning of the contraction, where the tunnel radius has decreased only to 8.705 inches, from 8.750 inches in the driver tube [13].

One of the possibilities for generating noise is free convection in the nominally stagnant driver tube air, prior to the beginning of the run. If free convection exists and sets up significant nonuniformities in the air, they could convect downstream once flow has begun, and cause early transition. Previous hot-wire measurements showed a significant level of seemingly random fluctuations in the flow leaving the contraction [13], and later measurements showed significant hot-wire voltage fluctuations before flow was initiated. It was thus necessary to determine if the pre-run fluctuations were due to free convection in the contraction, free convection due to the difference in temperature between the heated hot wire and the cooler tunnel air, or fluctuations due to a generally nonuniform tunnel temperature.

Hot-Wire Calibration

The hot wire used to measure disturbances in the entrance to the contraction needed to be calibrated in order to quantify the effects of disturbances in the contraction and the contraction boundary layer. The difficulty with performing the otherwise simple calibration is the changing density in the driver tube/contraction.

The low Mach number flow in the contraction would normally be modeled by King's Law:

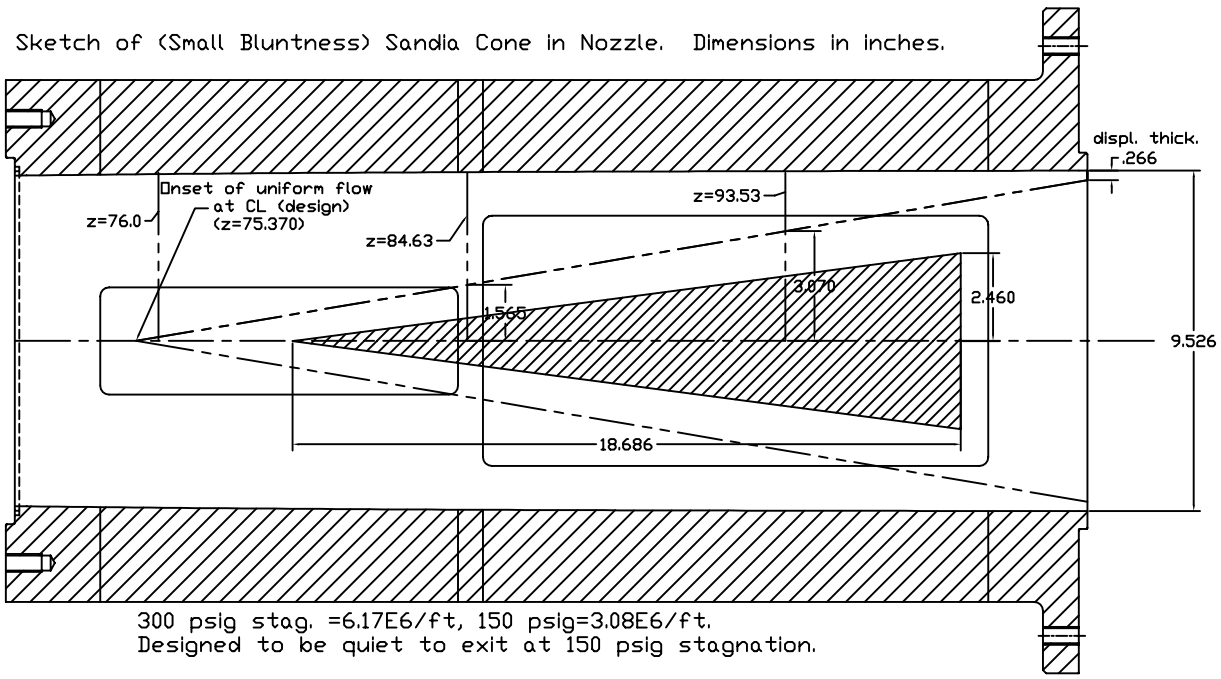

Figure 2: Schematic of Mach-6 Quiet Nozzle with Model

$$Nu = A\sqrt{Re_w}$$

where A and B are empirical constants, Nu is the Nusselt number, and Re_w is the wire Reynolds number. The changing density in the contraction, however, makes the use of this relation uncertain. It has been difficult to find literature showing calibrations with varying air density at low Mach number, although calibrations carried out for hot-wires at various altitudes on low-speed aircraft suggest useful precedents that are to be investigated [16, p. 4-22ff].

The initial stagnation temperature was set the same for all runs, 160°C. One hot wire, Platinum/10% Rhodium (Pt/Rh), was used for all runs. It had a diameter of .00015 in. and a length/diameter ratio of approximately 304.

All measurements used the standard bridge of an IFA100 constant temperature anemometer (CTA), in conjunction with an 8-bit Tektronix TDS7104 digital oscilloscope. The oscilloscope was operated in Hi-Res mode whereby data were sampled at 1GS/sec and then averaged into memory at the set sampling rate. All runs were sampled at 200KS/sec. An overheat ratio of 1.46 was used for the first calibration and an overheat ratio of 1.42 was used for the second calibration.

The hot-wire probe was inserted into the contraction section of the tunnel via the 1 in. instrument port on the top wall of the tunnel, where the contraction radius is 8.705 in. The probe's distance from the contraction wall was varied by adjusting a lead-screw traverse. For most runs, the hot wire was placed on the centerline of the tunnel. After the tunnel was pressurized to the desired initial stagnation pressure, the air was allowed to equilibrate for approximately 10 minutes before a run was initiated.

The nominally uniform flow in the contraction entrance was used to calibrate the hot wire. Calibrations were obtained for various densities by setting the initial stagnation pressure to 15, 30, 45, 75, 90, 105, 120, 135, and 145 psia. At each pressure, one run was made using the bleed suction and one was made with the bleeds closed. This provided slightly different Mach numbers in the contraction, due to the change in throat area and massflow. It was hoped that by recording both the actual contraction-wall static pressure and the CTA output during a run, a calibration relating CTA output to mass flow could be established via a Nusselt number/Reynolds number relationship.

Nusselt number was calculated from the hot-wire voltage. Mass flow, used in the Reynolds number, was found by assuming one-dimensional isentropic flow, using the formula

$$\rho U = PM\sqrt{\frac{\gamma}{RT}},$$

where ρU is the massflow. The static pressure, P, was determined using the transducer in the 3-inch access

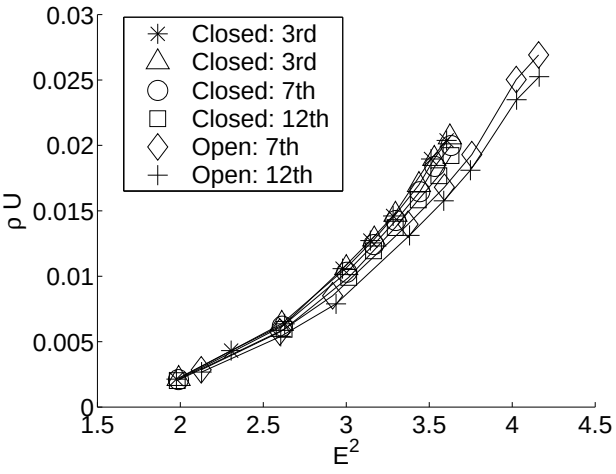

Figure 3: Hot-wire calibrations after 3rd, 7th, and 12th reflection of the expansion wave

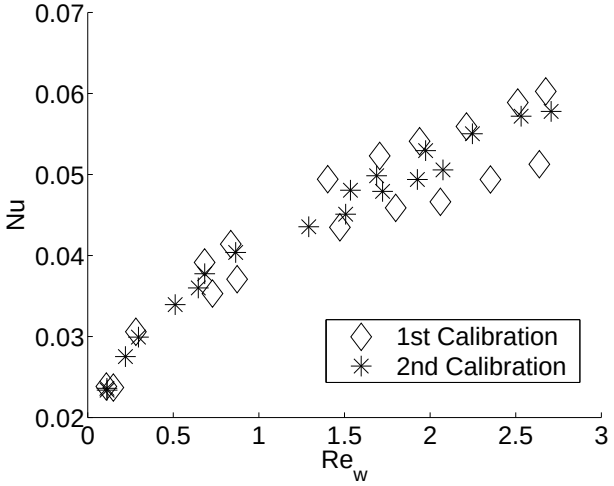

Figure 4: Hot-wire calibrations, boundary layer not modeled

port on the opposite contraction wall at the same axial station. The static temperature, T, was nearly equal to the initial stagnation temperature since the contraction entrance Mach number is about 0.003 [17]. The Mach number was found by using the one-dimensional isentropic area relation. The contraction area as well as the throat area are precisely known; boundary-layer thicknesses and possible separations were initially neglected. When the throat bleed slots were opened, a 38% increase in throat area was used in Mach number calculations, in agreement with simple estimates and also precision Navier-Stokes analyses [15].

Figure 3 shows the results of a sample calibration. Mass flow is plotted against the square of the hot-wire voltage. In order to ascertain the effects of pressure and the time from the beginning of the run, calibration calculations were made using three different quasi-static periods, after the 3rd, 7th, and 12th reflections of the driver-tube expansion wave. This was done for the bleeds both open and closed. In the case of the third period, the bleeds were not yet open because they generally take one to two seconds to fully open, and the wave period is approximately 200 ms.

Figure 3 shows that the calibration curves for runs with the bleeds closed matched quite nicely. Calibrating at a different time appears to have little effect. When the bleeds were opened, and the contraction-entrance Mach number was increased, the calibration shifts somewhat. It is possible that this is due to an error in the estimate of the contraction-entrance Mach number for the two cases, since boundary-layer separation was neglected in the throat, and is likely when the bleeds are closed.

Two additional calibrations were made for the same hot wire, as shown in Figure 4. Here, Nusselt number is plotted against the wire Reynolds number, as Nusselt number will be used to calculate mass flow. Both calibrations follow the same general trend. In both cases, the bleeds-open data is markedly above the bleeds-closed data (especially for the first calibration), again probably due to separation over the bleed lip when the bleeds are closed, and the corresponding error in computing the true massflow. Since most tunnel runs are made using the bleeds, and the theoretical massflow computation is less uncertain for this case, it was decided to calibrate using only the data with the bleeds open. The upper set of bleeds-open data repeats well for the two calibrations.

The effects of the contraction-entrance boundary layer were then considered. A simple Blasius model was used to estimate boundary layer thickness in the contraction. The 99% thickness was used in place of the displacement thickness due to an oversight, so the displacement-thickness effects are here overestimated. The fetch was taken to be a time-dependent distance found by multiplying the time with the speed of the passing expansion wave that initiates a run. Figure 5 shows the effect of this crude boundary-layer estimation. As can be seen, modeling the boundary layer shifts the calibration curve down slightly, but the effect is not large. Several simplifying assumptions were made in this crude model of the boundary layer. First, a constant temperature and density were assumed in the driver tube, although both drop throughout a run. Also, the time-dependent fetch does not model the complex effects due to expansion-wave reflections.

Preliminary calibrations were performed by plotted the Nusselt number vs. the Reynolds number, with

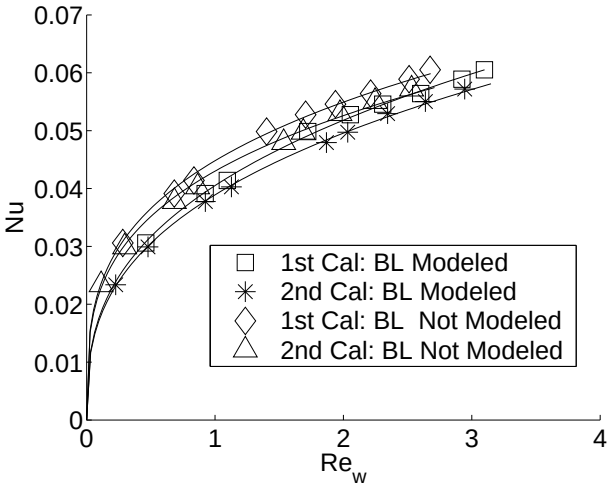

Figure 5: Calibration with and without boundary layer modeled

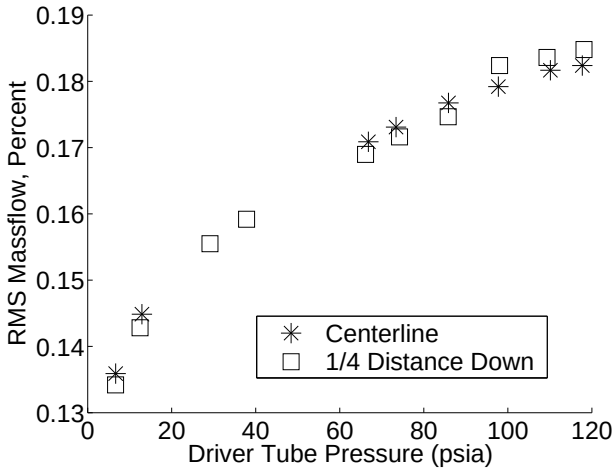

Figure 6: Average percent RMS noise levels along centerline and at half a radius down from the upper contraction wall

the boundary-layer effects included. It was thought that the crude model for these effects was better than neglecting them altogether. The second set of calibration data was used for the present analysis. Fig. 5 shows that this data was in good agreement with the power-law fit of

$$Nu = 0.0389 Re_w^{0.3496}.$$

RMS Fluctuations in the Contraction Entrance

This preliminary calibration was then used to find the percent RMS mass flow fluctuations in the contraction. The Nusselt number was obtained from the CTA output voltage. The curve fit was then used to back out the hot-wire Reynolds number and hence the mass flow.

If the mass flow fluctuations in the contraction were large enough, they could convect downstream and augment tunnel noise or even trip the nozzle-wall boundary layer to turbulent. To examine this risk, the normalized mass flow fluctuations in the contraction need to be compared to similar data obtained in the settling chambers of previous quiet tunnels. For example, Beckwith measured 0.2% velocity fluctuations in the settling chamber of the successful Langley Mach 3.5 quiet tunnel [18].

Figure 6 shows the fluctuations in massflow normalized by the mean, in percent. Here, the percent RMS is the average taken over a three second period from two until five seconds and is shown both on the tunnel centerline and at one half of a contraction radius down from the top tunnel wall. This generally captured data taken only after the bleeds were completely opened. In several low-pressure cases, the bleeds did not fully open until about three seconds into the run. In these cases, the start time for the averaging was increased until after the bleeds were fully open.

As can be seen, the maximum noise level is less than 0.19% and drops by approximately 30% to 0.13%. This is expected as the higher density makes larger mass flow fluctuations for equal velocity fluctuations. Both vertical locations give very good agreement for average RMS noise, suggesting the noise is fairly uniform. The levels are comparable to those measured by Beckwith in the settling chamber of the Langley Mach 3.5 quiet tunnel [18, p. 229], suggesting they are significant but acceptable. Further study is clearly in order.

Contraction Boundary Layer Measurements

A preliminary investigation of the contraction boundary layer was undertaken as well. The previous freestream calibration does not hold within the boundary layer since Mach number, temperature, etc., all vary from freestream values. Nevertheless, a qualitative examination of the hot-wire voltage fluctuations was made.

Figure 7 shows the RMS fluctuations for locations from 0.02 in. to 0.30 in. in steps of 0.025 in. for different times after the start of a run. Each of the points were averaged over 0.25 seconds. The RMS noise closer to the wall was typically 2 to 3 times larger than those further away.

The RMS noise levels are expected to be highest at the edge of the boundary layer because the shear stress is highest there. If that criterion for the edge is used, the boundary layer only grows from 0.05 in. to 0.10 in. This is much less than for the Blasius boundary layer

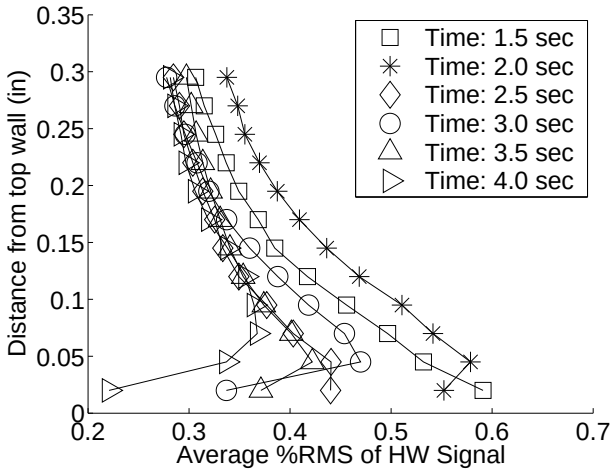

Figure 7: RMS noise taken in the boundary layer for various times

analyzed previously. The reason for the discrepancy is not yet understood.

Eighth Throat Insert

Brief Summary of Design

In an attempt to improve flow quality and quietness in the Mach 6 Ludwieg Tube, an eighth throat insert design was designed, fabricated and tested, following procedures similar to those used for the Case 7 design [11, 10]. The massflow was again increased, to a nominal value of 50% of the upstream flow, by increasing the slot width. This should move the stagnation point nearer to the main-flow side of the bleed tip, and reduce the risk of a separation bubble there, although it was recognized that the increased massflow might exceed the capabilities of the suction exhaust piping. Table 3 from Ref. [10] is again updated as Table 1; the symbols again have the same definitions as in Ref. [10]. A simple one-dimensional analysis predicts that the stagnation point is now 0.014 inches below the bottom of the 0.030-inch tip. Although this is clearly unphysical, the downward movement of the stagnation point should help to eliminate the separation bubble, if the necessary massflow can be supplied.

It was again noted that the Beckwith bleed-lip designs have a much larger angle with respect to the contraction wall, so the angle was increased by an amount that was 2.0 degrees for Cases 7 and 8. A larger angle could not be used while still maintaining monotonic slopes in the contraction contour. Although the case 8 geometry is already not quite monotonic in slope,

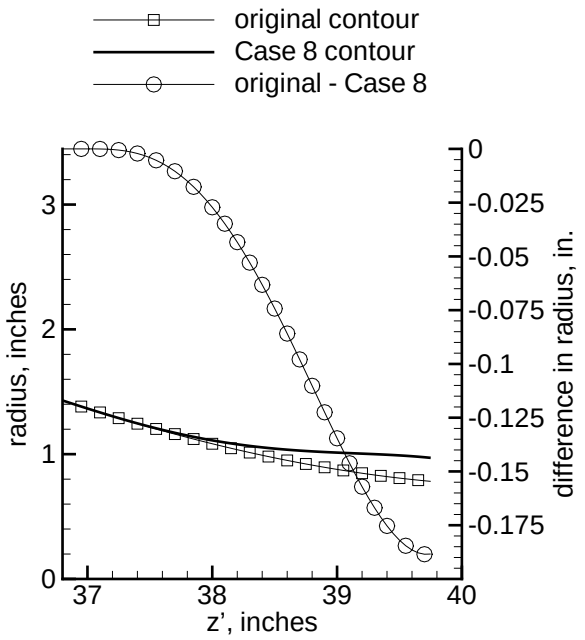

Figure 8: Modification to Contraction Contour, Case 8

the concave region is essentially within the slot area, so any disturbances generated there should be swept into the slot. Fig. 8 shows the modification to the geometry. The horizontal axis, z', is the axial contraction coordinate, where $z' = 0$ at the contraction entrance. The modifications were made to an insert that picks up the contour at $z' = 37.0$ in. The contour again makes a smooth joint at the match point, with a larger radius downstream, and with the difference in radius increasing monotonically.

Fig. 9 shows a drawing of the new geometry. The upstream joint with the stainless-steel contraction section should be nearly flush. It should be noted that the Case 6, 7, and 8 designs have the bleed lip moved upstream 0.250 inches compared to the earlier designs.

Preliminary Experiments

The tunnel was cooled in order to open up the throat section and substitute the insert. After the insert was secured and the tunnel closed, it was heated again to 160°C. The temperature was allowed to equilibrate overnight before any runs were made.

A Kulite pitot pressure transducer on the tunnel centerline located at $z = 76.42$ in. measured pitot pressure. The AC, DC, and temperature-compensator voltages were recorded. Additional pressure measurements were recorded from two Kulite static pressure

Case:	1	2	3	4	5	6	7	8
entry, in.	0.036	0.036	0.036	0.073	0.073	0.1088	0.161	0.244
min. in.	0.029	0.029	0.036	0.042	0.062	0.1014	0.146	0.229
A_{entry}/A^*	1.24	1.24	1.0	1.74	1.18	1.073	1.10	1.07
P_{se}/P_t	0.81	0.81	0.53	0.91	0.78	0.70	0.73	0.70
$h_e(P_e/P_t = 0.82)$, in.	0.037	0.037	0.046	0.053	0.079	0.1288	0.185	0.288
$h_{e,tip}(0.82)$, in.	0.001	0.001	0.010	-0.020	0.006	0.020	0.024	0.044

Table 1: Properties of Bleed-Slot Geometries

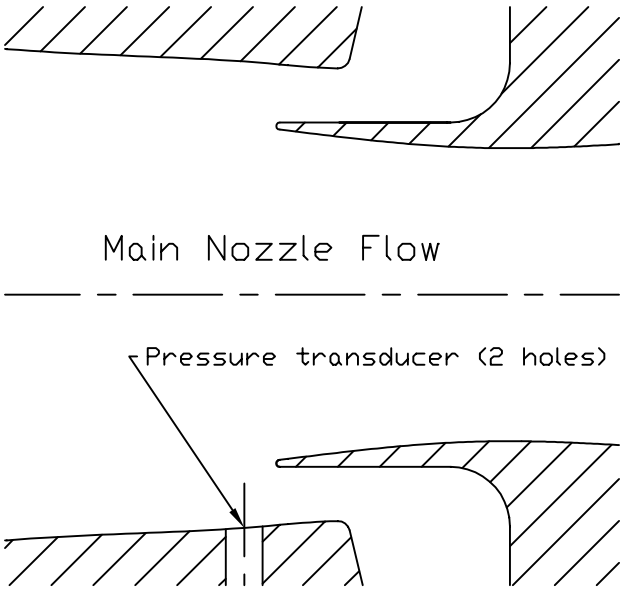

Figure 9: Drawing of Slot Throat, Case 8

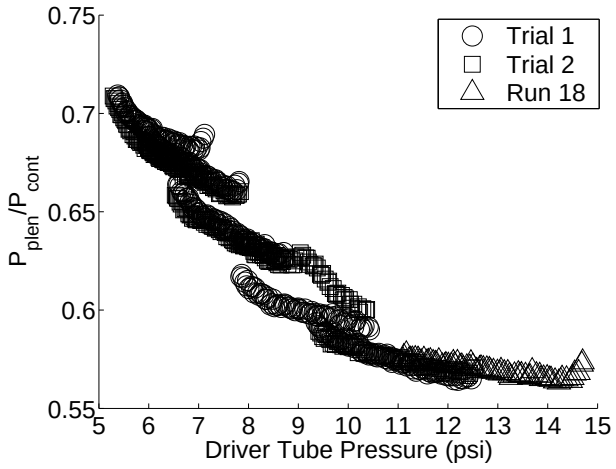

Figure 10: Ratio of static pressures in the plenum and contraction

transducers located in in the bleed slot throat at the same axial location, with azimuths differing by 135 deg. Pressure measurements were also obtained in the contraction entrance and in the bleed-slot suction plenum.

All the signals from the pitot probe and the bottom throat transducer were recorded on an 8-bit Tektronix TDS7104 digital oscilloscope operating in Hi-Res mode. The bottom throat transducer AC signal and side throat transducer DC and AC signals were recorded on a LeCroy 9314AL digital oscilloscope at a sampling frequency of 100kHz. The contraction and plenum DC signals were recorded on a LeCroy 9304AM digital oscilloscope at a sampling frequency of 25kHz. All oscilloscope records were 10 seconds long.

The key result is shown in Figure 10, which plots the pressure ratio between the suction plenum and the driver tube (the suction plenum is downstream of the bleed slot). This ratio never drops below the maximum value of 0.528 necessary for sonic flow in the bleed-slot throat, probably because the massflow is too large for the suction piping. The possibility that sonic flow remains due to a supersonic pressure recovery in the plenum appears remote. However, this possibility cannot be precluded due to a calibration problem with the throat Kulites.

The effect of the poor suction-slot flow is also evident in Figure 11, which shows the Mach number in the nozzle; the values are very close to 6, as expected, once the temperature correction for the Kulite was taken into account. Large variations are present during each run, probably due to variations in the poorly controlled suction-slot flow.

Figure 12 shows the RMS of the mean pressure recorded by the pitot transducer, in percent. The pre-run RMS has been subtracted off by finding the square root of the difference of the squares of RMS and pre-run RMS. As can be seen, the RMS fluctuations are quite large, perhaps because of the poor slot flow. With this throat insert the tunnel was not operating at typical RMS levels for the typically quiet flow below 8 psia. It should be noted that at low pressures, turbulent spikes disappeared from the DC pitot traces.

Figure 13 shows the RMS as a percentage of the mean for both throat Kulites. There was an unknown

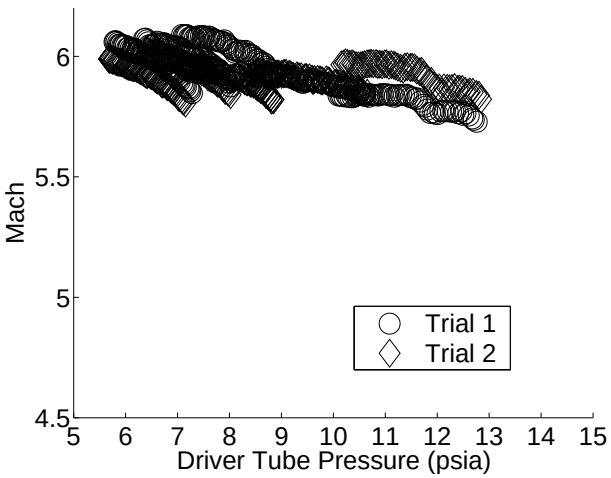

Figure 11: Mach number vs. driver tube pressure on centerline

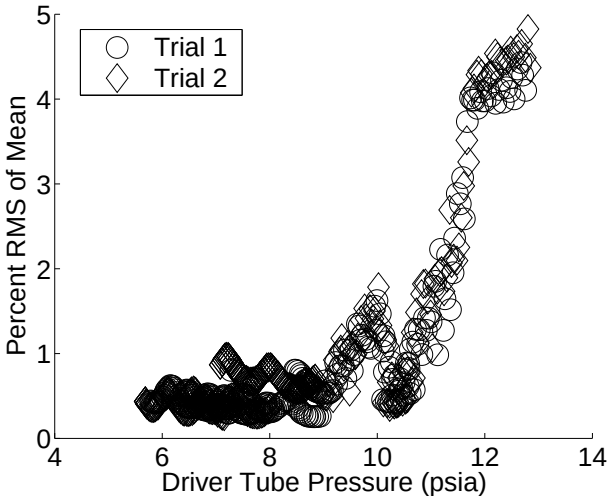

Figure 12: Percent RMS pitot pressure fluctuations

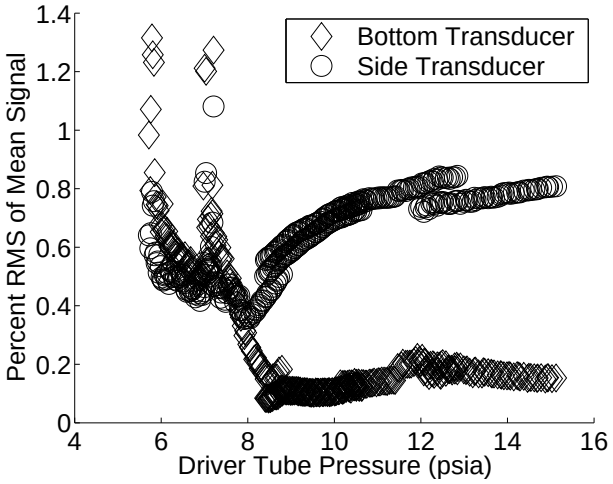

Figure 13: Percent RMS of throat signal

problem with the calibration of these Kulites, so quantitative data could not be reported, limiting the utility of the data collected. The figure nevertheless shows clearly that the Kulite fluctuations are much different on the two sensors. This is probably due to asymmetry in the suction through the bleed slot. This would lead to a highly complex, unsteady, and presumably noisy flow field. Additionally, the resulting disturbances could feed forward through the subsonic portions of the flow and pollute the flow entering the main nozzle of the tunnel, adding additional noise to the flow.

It thus appears that the eighth bleed-slot design overshot the allowable suction massflow and failed to achieve sonic flow in the bleed-slot throat. This insert was removed after this test, and the Case-7 insert was reinstalled. Future insert designs will need a smaller suction-throat area than was attempted in Case 8.

Initial High Reynolds Number Operations

Motivation

Crossflow and roughness-induced transition are to be studied on blunt-nosed cones at angle of attack [1, 13]. To obtain information on the transition mechanisms, affordable transition data is in many cases desirable. The Boeing/AFOSR Mach-6 Ludwieg Tube is rated for a maximum stagnation pressure of 300 psig, but is presently only operated up to about 130 psig. A boost pump has been added to enable us to reach the higher stagnation pressures, so that conditions for transition on blunt cones can be approached [14].

Boudreau Experiments Re
Nosetip Roughness Effects

Roughness can form on the surface of a re-entry vehicle as the heat shield material ablates, and there is initial roughness as well. This roughness may be a primary cause of transition in the boundary layer over the vehicle [19, 20]. Ref. [1] noted in passing that windside-forward transition on blunt cones at angle of attack appears to be associated with nosetip roughness.

Recently the authors became aware that A. H. Boudreau of ARO, Inc. also studied frustum transition caused by distributed roughness on the noses of slender cones [21, 22, 23]. Boudreau's experiments were carried out to improve methods of fixing boundary layer transition by attaching tripping elements to the surface of a wind tunnel model. Spheres were a standard tripping element because they offered uniformity of size and shape and ease of application. However, such large, individual elements often extended outside the boundary layer and caused flow disturbances felt far downstream that would not be encountered in flight. It was thus desirable to investigate distributed roughness, a series of smaller elements distributed around the surface of a vehicle, as a tripping mechanism that would not create such large disturbances in the flowfield. Distributed roughness is also of interest because it approximates a likely roughness condition for reentry vehicles in flight.

Boudreau used a 7-deg. half-angle cone with a 48-in sharp-cone length [21, 22]. The stainless steel model had ten interchangeable nosetips that varied in bluntness and roughness configuration. Surface heating was measured with thermocouples. Experiments were conducted in AEDC Tunnels B and F. The tunnel F model had pressure transducers to measure the pressure at the surface of the model. Shadowgraphs were taken in Tunnel F to visualize the flowfield disturbances caused by the roughness elements.

Spherical trips were compared to various distributed roughness configurations. The distributed configurations were created by blasting the nosetip with grit, applying grit to the nosetip, and machining pyramidal structures into an aluminum nose. The first two methods can be easily reproduced at the Aerospace Sciences Lab at Purdue University.

Boudreau found that distributed roughness elements only one-fifth as tall as spherical elements tripped the boundary layer without causing large disturbances to the flowfield over the cone, as seen in shadowgraph photos. He also found that distributed roughness elements applied forward of the maximum local Reynolds number location (about 45-deg. from the stagnation point) on the hemispherical nose were less effective than those applied downstream of it. Also, he found that roughness elements should extend all the way to the 'pressure bucket' to maintain turbulence. Boudreau theorized that the leading roughness elements, positioned in the thinner boundary layer at the front of the nose, trip the layer, while the downstream roughness elements maintain turbulence against potential laminarization due to the favorable pressure gradient over the shoulder of the nose. Distributed roughness configurations using 14- to 25-mil roughness elements on a 0.589-in.-radius nose at Mach 8 brought the end of transition to $s < 10$ inches for $2 \times 10^6/\text{ft} < \text{Re}_\infty < 4 \times 10^6/\text{ft}$ [21, Fig. 11],where s is the distance from the stagnation point along the surface of the model. Boudreau also noted an increase in transition distance with increasing freestream Mach number [21, pp. 17-18].

These results indicate that experiments for transition induced by distributed roughness are likely to be feasible on the 12- to 18-inch models that can be tested in the Purdue Mach 6 Ludwieg tube at $Re_\infty < 6 \times 10^6/\text{ft}$. An aluminum 7-deg. cone model has been built that uses interchangeable nosetips of varying nose radii. Distributed roughness elements can be applied to the nosetips with adhesive or by sandblasting. Transition can be detected through the use of temperature sensitive paint on the frustum. Hotwire studies of instabilities in the boundary layer may also be carried out. The effects of roughness element type, size, and distribution on transition at Mach 6 can be investigated.

Porthole Window

Although the Mach-6 tunnel was built to allow 300 psig operation, existing instrumentation has only been tested to about 150 psi. In particular, the large acrylic window used for oil-flow visualization and temperature-sensitive paints is only rated to 138 psig [24]. Since these techniques are critical to effective study of transition induced by roughness and stationary crossflow waves, a porthole window was designed and built to provide optical access at higher pressures. A portion of the assembly drawing is shown in Fig. 14. The stainless-steel insert fits the large 7x14-inch openings in the last section of the nozzle, just like the present rectangular window. The smaller 5-inch dia. circular openings provide similar safety factors at higher pressures. Acrylic is again used, despite its reduced optical clarity compared to glass, because it is a ductile material that is much less sensitive to stress concentrations and cracking [25, 26]. It is also much less expensive to procure and machine. High quality ASTM-D-5436 UVT cast acrylic in the stress-relieved condition permits good transmissivity

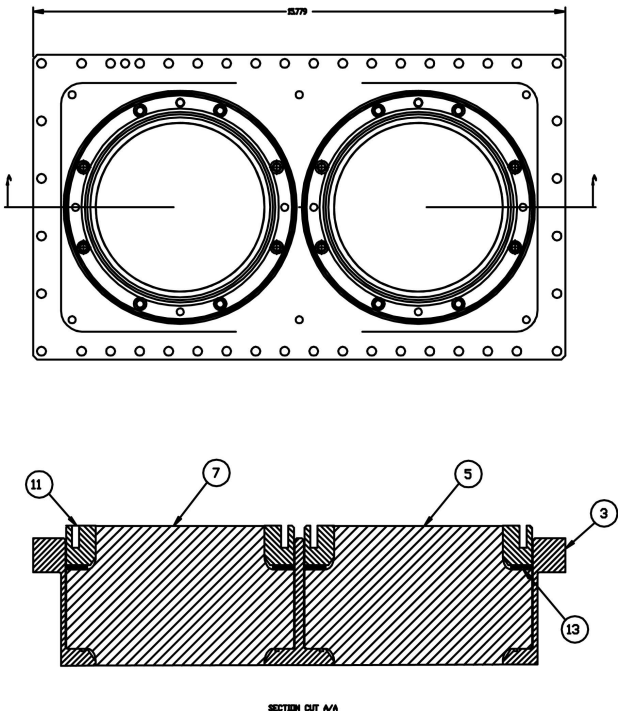

Figure 14: Viewport from Drawing of Porthole Window

well into the blue part of the spectrum, as is needed for the temperature-sensitive paints. Ref. [25] reports that acrylic plastic showed visible cracks well before repeatable failures in cyclic loading (pp. 427-428), in marked contrast to glass, which provided no notice of sudden and poorly reproducible failures (p. 437-448).

This proven ductility [25, p. 424] was used to justify a much less detailed stress analysis than was used for the rectangular window. The vendor carried out two axisymmetric finite-element stress analyses for the window [27]. For the finer grid with 16402 elements, the peak stress of 910 psia occurred in bending at the radiused corner where the plexiglas bears on the retaining ring. This provides a safety factor of about 10, which is very conservative, and does not even include the stress-relieving effect of the babbitt-metal gasket used to distribute this stress concentration.

Effect of Downstream Disturbances on Upstream Noise

Initial Hot-Wire Measurements in the Nozzle Boundary Layer

Measurements are being made in the boundary layer to get direct data about the flow near the wall.

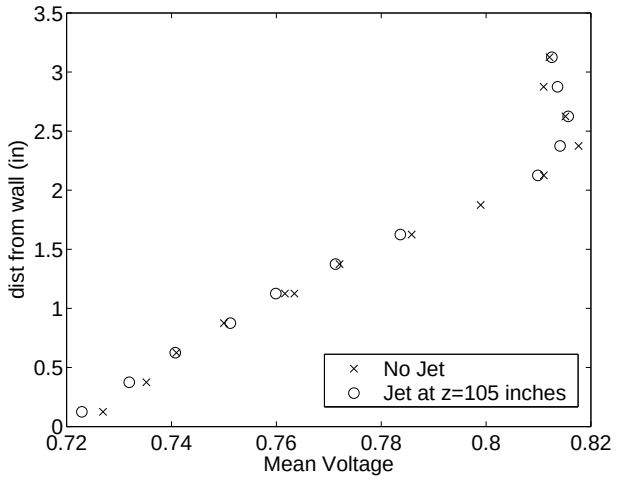

Figure 15: Boundary layer profile with an initial pressure of 8 psia with turbulent boundary layer

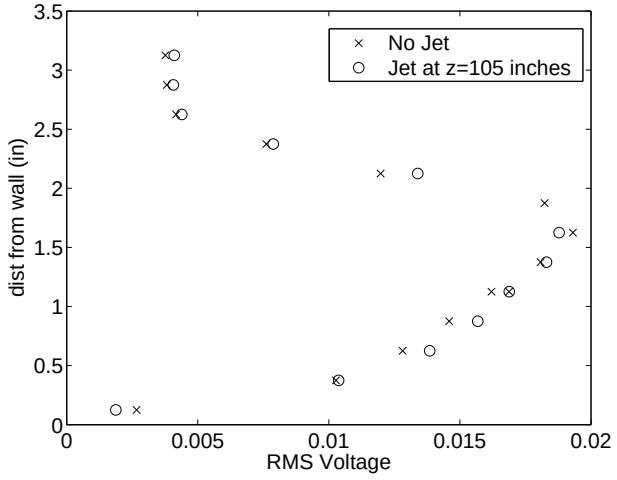

Figure 16: RMS fluctuations with an initial pressure of 8 psia with turbulent boundary layer

Most of the data that was obtained previously and the data shown in the next sections use pressures measured on the tunnel centerline. This only indirectly shows what is happening at the tunnel walls far upstream. The advantage of the data measured at the centerline is that it allows a simple overview of what is occurring in the tunnel at a large range of pressures.

Uncalibrated hot wire measurements were made with a constant-temperature anemometer at high overheat, in the boundary layer on the bottom wall of the tunnel at $z = 84.3$ inches, where z is the axial distance downstream of the throat. Profiles were made with and without a transverse sonic jet, through a 1/4-20 inch hole, in the diffuser at $z = 105$ inches. Figure 15 shows profiles for runs with the bleeds closed, with an

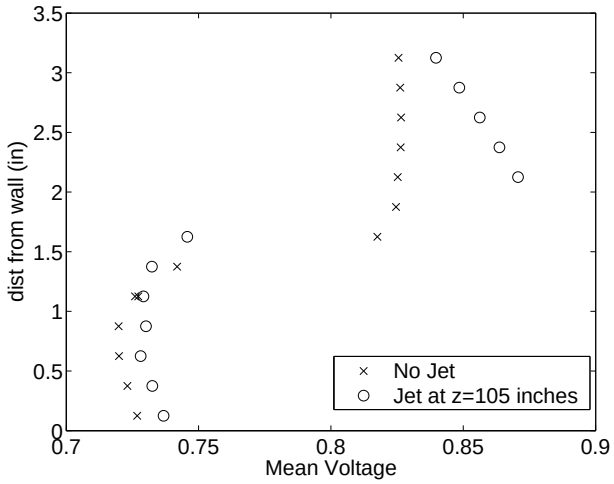

Figure 17: Boundary layer profile with an initial pressure of 8 psia with laminar boundary layer

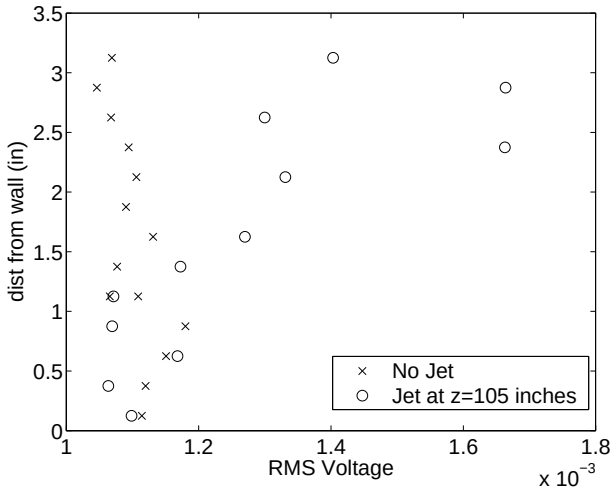

Figure 18: RMS fluctuations with an initial pressure of 8 psia with laminar boundary layer

initial driver tube pressure of 8.01 psia ± 0.3% without the jet and 7.99 psia ± 0.4% with the jet. For these pressures, centerline probe data at $z = 75.3$ inches show noisy flow with the bleeds closed. This indicates turbulent flow at the tunnel walls, upstream at the acoustic origin. The acoustic origin is the location at the tunnel wall upstream where disturbances can follow Mach lines to the center of the tunnel where the probe is located. The mean driver tube pressure during the averaged time period of 0.5 to 0.6 seconds after the run start was 7.81 psia ± 0.4% without the jet and 7.77 psia ± 0.4% with the jet. This figure shows that the jet has no effect on the boundary layer at this location. It is likely that disturbances from the jet are unable to feed forward through the turbulent boundary layer. Figure 16 shows the RMS fluctuations for the same runs. This shows no effect of the jet on the noise levels seen in the boundary layer.

Figure 17 shows the profiles for runs with the bleeds open, with an initial driver tube pressure of 8.01 psia ± 0.3% without the jet and 7.99 psia ± 0.4% with the jet. For these pressures, centerline probe data at $z = 75.3$ inches show quiet flow, suggesting a laminar upstream boundary layer. The mean driver tube pressure during the averaged time period of 3.0 to 3.1 seconds after the run start was 6.83 psia ± 0.5% without the jet and 6.83 psia ± 0.6% with the jet. This figure indicates that there is a laminar separation with and without the jet present in the diffuser. Figure 18 shows the RMS fluctuations for the same runs. This shows there is similar noise in the separated region for both cases, but for the case with the jet the noise is larger outside of the separated region. This may indicate that even though the flow is separated, the jet is still able to disturb the core flow more than the separated flow does without the jet.

Figure 19 shows the profiles for runs with an initial driver tube pressure of 14.40 psia ± 0.4% with and without the bleeds open. For these pressures, centerline probe data at $z = 75.3$ inches show noisy flow with or without the bleeds open, showing that the upstream boundary layer is turbulent. The mean driver tube pressure during the averaged time period of 0.5 to 0.6 seconds after the run start for the bleeds closed profile was 14.07 psia ± 0.4%. The mean driver tube pressure during the averaged time period of 3.0 to 3.1 seconds after the run start for the bleeds open profile was 12.29 psia ± 0.7%. This figure shows that the boundary layer is nearly unchanged between the two cases. The slight offset is likely due to the difference in driver tube pressure rather than any change due to the effects of the bleeds. Figure 20 shows the RMS fluctuations for the same runs. This again shows little effect from the operation of the bleeds. This indicates that for operation above 10 psia, where the tunnel is noisy, the flow is the same whether the bleeds are open or closed, because in both cases the boundary layer is turbulent and resistant to separation.

Disturbances Caused by Shock Impinging on Nozzle Wall

Disks of 1.5 and 3-inch diameters were placed at $z = 101.7$ inches to cause shocks that impinge on the wall and create shock/boundary layer interactions. Pitot Kulite measurements were taken on the centerline at $z = 75.3$ inches. These measurements were taken with the new sting mount as described in Reference [11]. Figure 21 shows a diagram of the location

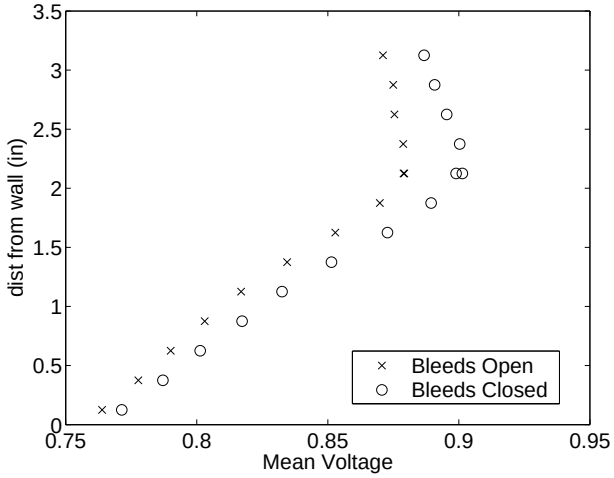

Figure 19: Boundary layer profile with an initial pressure of 14 psia with turbulent boundary layer

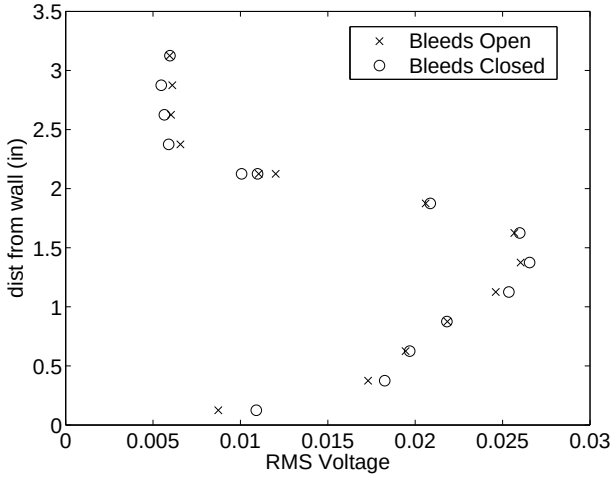

Figure 20: RMS fluctuations with an initial pressure of 14 psia with turbulent boundary layer

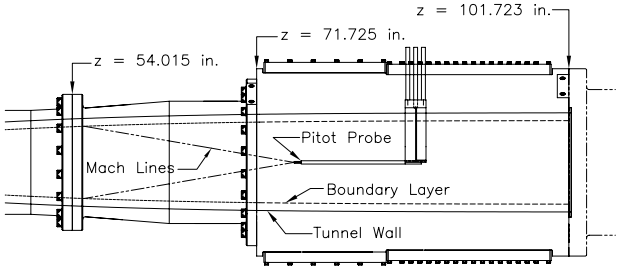

Figure 21: Diagram of Pitot probe in end of nozzle

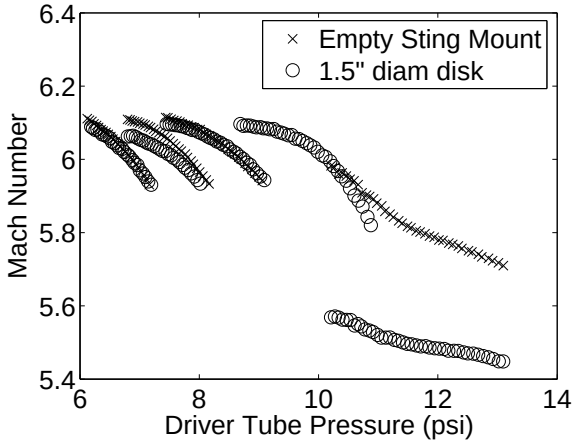

Figure 22: Effect of 1.5-inch diameter disk on Mach number

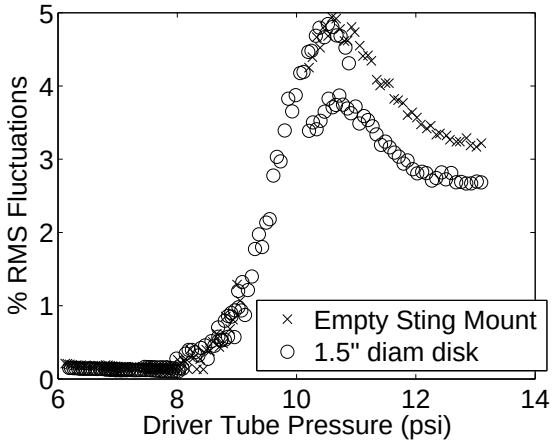

Figure 23: Effect of 1.5-inch diameter disk on RMS fluctuations

of the Pitot probe in the nozzle. The disks were placed near the right side of this diagram. The Pitot probe only indirectly shows what is occurring in the boundary layer upstream of the probe. Any disturbances in the boundary layer will be transmitted to the center of the tunnel along Mach lines until they reach the Pitot probe at the center of the tunnel.

Figure 22 compares the effect of a 1.5 inch diameter disk to the control case with an empty sting mount. The initial driver tube pressures for the data taken with the empty sting mount were 8.01, 9.01, 10.01, 11.98, and 14.50 psia. The initial driver tube pressures for the data taken with the 1.5-inch diameter disk were 8.02, 9.01, 10.01, 12.01, and 14.47 psia. For each run, the data is averaged over 0.1 second intervals as the pressure drops throughout the run. This allows data to be gathered over a range of driver tube pres-

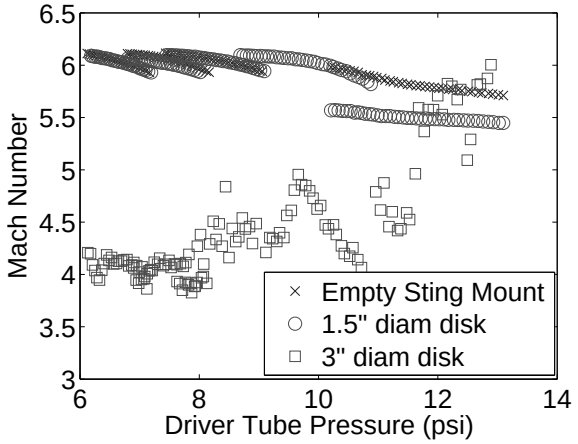

Figure 24: Effect of 3-inch diameter disk on Mach number

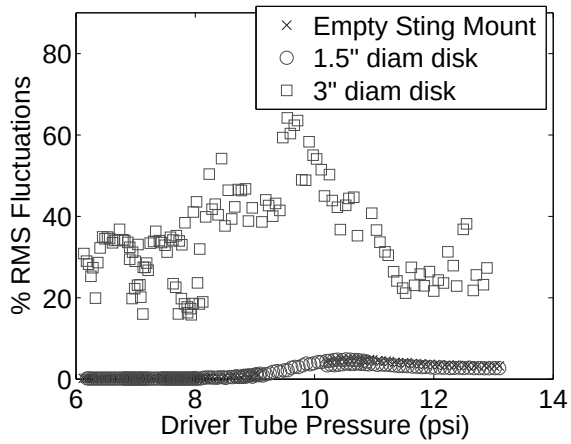

Figure 25: Effect of 3-inch diameter disk on RMS fluctuations

sures during a single run. The data shown in the plots start at significantly lower pressures due to the approx. 2 sec. wait for the bleed system to open. The Pitot probe shows a lower Mach number for the run with an initial driver tube pressure of 14.47 psia with the 1.5 inch diameter disk, but not for the lower pressure runs. This indicates a possible separation upstream at the acoustic origin.

As shown in the boundary layer profiles in the previous section, the boundary layer is separated going into the diffuser for low pressures. This is not evident as a reduction in Mach number for this data at the centerline, because the separation occurs downstream of the acoustic origin for this probe placement. Since there is an attached turbulent boundary layer at higher pressures, Figure 22 indicates that the shock impinging an already separated flow has less upstream effect than the shock impinging on an attached turbulent boundary layer, as expected. Figure 23 shows the RMS fluctuations for the same data. The fluctuations do not appear to be affected by the disk. The higher pressure data with the disk shows lower fluctuations only because it is nondimensionalized by a higher pressure since the flow is separated.

Figure 24 and Figure 25 add the data using the 3-inch disk to the data shown in Figure 8 and Figure 9. The initial driver tube pressures for the data with the 3-inch disk were 8.00, 9.02, 10.01, 12.01, and 14.48 psia. The 3-inch disk causes a stronger shock that would be expected to have a larger effect on the boundary layer. Figure 24 shows that the 3-inch disk causes large upstream separations. This could be an indication of an unsteady unstart of the tunnel.

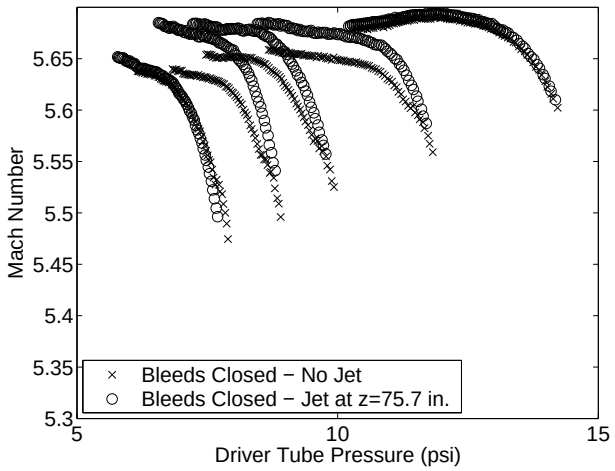

Figure 26: Effect of a disturbance on Mach number with bleeds closed

Effects of Transverse Sonic Jets

The initial measurements of transverse sonic jets were reported in Reference [14]. These showed that jets added to the tunnel can have a large effect on the flow upstream of the jet. Additional measurements were performed with the bleeds closed to examine the effects of a turbulent boundary layer with and without a jet disturbance downstream.

Before the new bleed system, there was always a disturbance downstream where the jets from the bleed system fed back into the tunnel, except when the tunnel was operated with the bleeds closed. The disturbance that was used here was created by removing a 1/4-20 inch bolt at $z = 75.7$ inches. This is not as large of a disturbance as the original bleed system created, but it is much farther forward. The Pitot probe

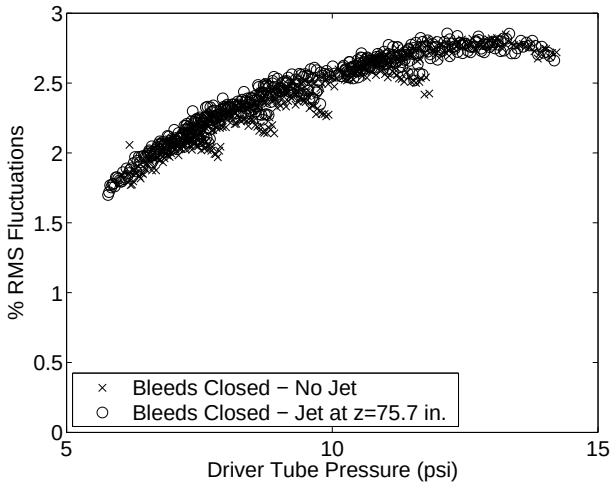

Figure 27: Effect of a disturbance on noise with bleeds closed

was located only slightly forward of this at $z = 75.3$ inches. Figure 26 shows the Mach number with and without the disturbance. The initial driver tube pressures for the data with no jet were 7.99, 8.99, 10.00, 11.97, 14.47, and 14.50 psia. The initial driver tube pressures for the data with the jet were 8.06, 9.08, 10.11, 12.05, and 14.50 psia. There is little difference between the data with and without the jet. The Mach number does rise by about 2-3% throughout each run. This effect has been noticed before, but seems to be larger in this case. It is believed to either be the result of changing conditions in the driver tube, such as a decreasing temperature as the pressure decreases, or an effect of calibration shifting of the Pitot Kulite pressure transducer as the sensor is heated during the run.

Figure 27 shows the noise for the same data. This shows all noisy flow as is expected with turbulent boundary layers. There is no difference between the data with and without the disturbance. This shows that the disturbance that caused a separation with a laminar boundary layer does not cause a measurable separation in a flow with a turbulent boundary layer. There is also no noticeable increase in the noise level, which indicates that any noise transmitted upstream does not significantly increase the noise already present in the turbulent boundary layer.

In all the cases studied so far, disturbances that are created in a laminar boundary layer cause separation upstream before they trip the upstream flow to turbulence. This suggests that downstream disturbances do not cause the early transition on the nozzle wall of the tunnel. However, work continues.

Summary of Quiet-Flow Development Issues

Possible causes of the early transition on the nozzle wall include:

1. Fluctuations generated at the nozzle throat due to problems with the bleed-slot flow. Computations reported in Ref. [15] make this the most likely cause at present.

2. A nozzle-wall temperature distribution that decreases much more rapidly downstream than was initially expected. However, computations suggest this effect should be minor, and there is no evidence to suggest it could cause transition in the way observed.

3. A 0.001-0.002-inch ($Re_k < 12$) rearward-facing step at the downstream end of the electroform [28]. Here, Re_k is a roughness Reynolds number based on the height of the peak roughness, and the conditions in a smooth-wall boundary layer at the roughness height. However, this step was dramatically reduced by the fall 2002 polishing, without noticeable effect [11].

4. Insufficient polish on the downstream nozzle sections (although $Re_k < 12$). However, the fall 2002 polish had no noticeable effect.

5. Fluctuations or nonuniformity in the driver tube flow that lead to early transition. The preliminary measurements carried out to date suggest that this is an issue, but probably not the cause of early transition.

6. Some fundamental problem with the use of a very long nozzle which is not captured by the e^N analysis. This seems unlikely, since transition seems to flash forward along the whole downstream half of the nozzle at about the same pressure [13].

7. Noise propagated upstream from the diffuser section. Measurements reported in Ref. [12] show that the original diffuser centerbody caused separation in the nozzle-wall boundary layer when it began to drop laminar. Measurements in the Langley Mach-6 quiet nozzle showed that transition flashed forward on a flared cone when the nozzle exit shock impinged on the aft end of the cone. Upstream propagation of disturbances remained a concern, even with the new model support design, due to the jets of air from the bleed-slot suction that enter the diffuser downstream. However, when jets were removed by plumbing this bleed air directly to the vacuum tank, there was no marked

effect [13]. In addition, more recent measurements seem to show that downstream noise separates an incoming laminar boundary layer before it causes transition.

8. Flaws in the throat-region polish. A small bump can be felt on the bleed lip, and it is possible that this bump is tripping transition. Some small superficial scratches have become visible recently, although the throat remains remarkable clean and free of oil deposits.

9. Leaks in the low-pressure sections that cause jets of air into the nozzle, tripping the boundary layer. Although testing with soap films while the nozzle was under pressure did not show such leaks, small leaks were still a concern. However, more sensitive leak tests were recently carried out with a helium sniffer, and these failed to show any leaks in the critical portions of the tunnel [29].

10. Vibrations of the bleed lip, introducing disturbances that trip the flow. The tunnel vibrates when the flow starts up, but although these vibrations can clearly be felt, they seem to damp within a second or two. However, the onset of transition seems to occur at the same pressure, regardless of whether this pressure is at the beginning or the end of a run, making this cause seem less likely. The Mach-4 tunnel did not have this problem, but it did not use throat suction either, and the bleed lips may be more sensitive to vibration, particularly in the transverse direction. Measurements of these vibrations are planned.

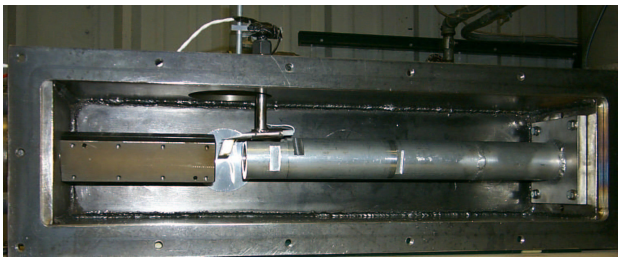

Figure 28: Supersonic jet with hot wire positioned at the centerline of the exit plane

Progress with the Hot Wire Measurements on Blunt Cones

Hot-Wire Calibrations

The hot wires are calibrated in the supersonic jet at the Purdue Aerospace Science Laboratory. A Mach 4 nozzle was designed and built for this purpose [30]. The Mach-4 nozzle allows for a continuous run with a 2.5-cm diameter test nozzle at approximately Mach 3.9. The stagnation pressure and temperature in the jet can be varied independently. The pressure in the plenum section is measured using an Ashcroft temperature-compensated test gauge with a range of 0-100 psia and an accuracy of 0.25%. The temperature in the plenum is measured with a Fluke thermometer and a J-type thermocouple.

To obtain accurate calibrations in the jet, the flow must first be characterized using Kulite pitot-pressure probes and cold-wire temperature sensors. The cold wire and Kulite probes can be placed in the center of the nozzle exit flow by using the traverse seen in Figure 28. Previously reported hot wire calibrations used the Kulite measurements obtained by P. Schneider [31].

The Mach and pressure profiles of the jet were obtained using a Kulite Pitot probe. The Kulite fast pressure transducer was placed in the center of the nozzle exit flow and connected to custom-built electronics. The stagnation pressure was then varied between 16.5 and 44.5 psia in 2 psi increments. A second set of data for this pressure range was then obtained to determine the repeatability of the measurements. The Mach number, mean Pitot pressure, and percent rms noise were then calculated and are plotted versus the plenum pressure in Figure 29. There is a significant drop in Mach number for pressures below 20 psia which was attributed to separation in the jet.

The RMS pitot fluctuations are now at a normal level of about 2% or less, showing that earlier problems with high fluctuation levels have now been resolved [13, p. 4]. It turned out that the joint at the throat

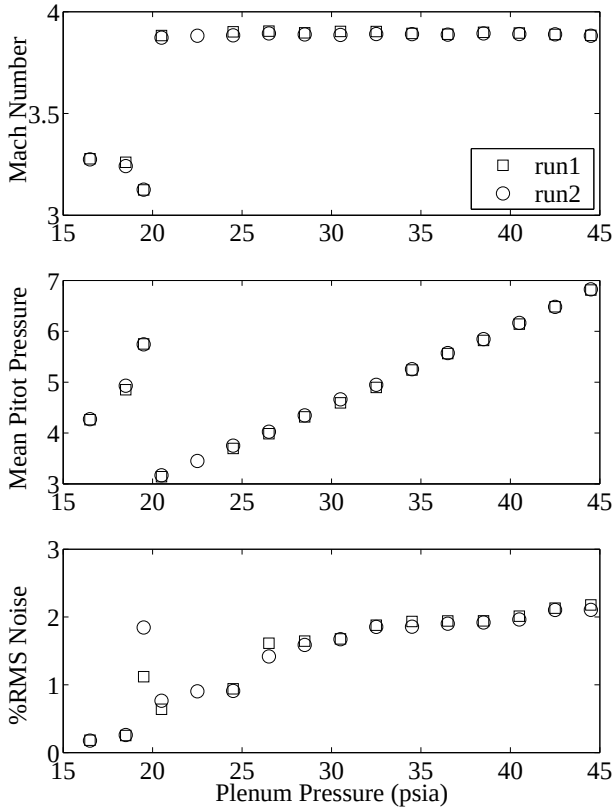

Figure 29: Kulite Measurements in the Supersonic Jet

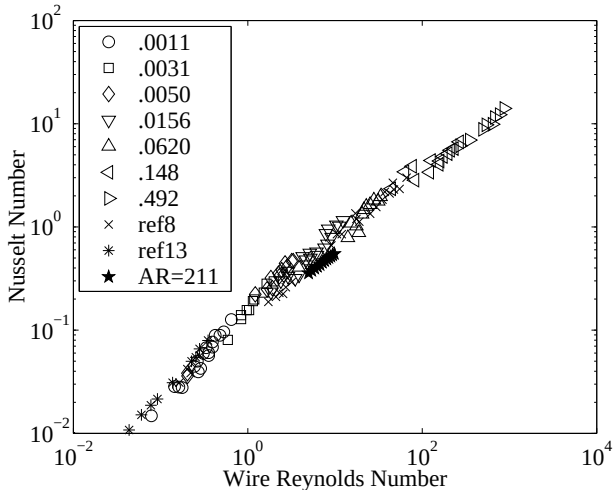

Figure 30: Nusselt/Reynolds number calibration curve comparison. Present data is 'AR=211', other data from Weltmann and Kuhns

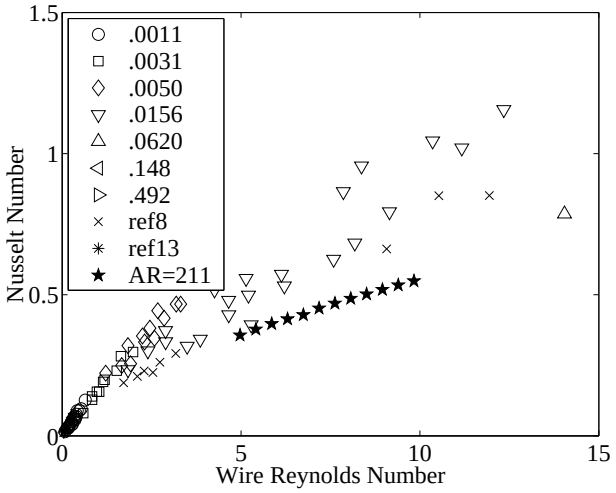

Figure 31: Close-up of the Nusselt/Reynolds number Calibration Curve

between the contraction and the Mach-4 nozzle had been poorly fitted, and introduced large steps and gaps at this critical location. After the parts were modified to provide reliably smooth flow surfaces, the high noise levels were eliminated.

A hot wire, HW1, was then placed in the jet on the centerline of the nozzle exit flow. The cold resistance of the wire was measured as 16.1 ohms, and the aspect ratio was 211. The hot wire was connected to a 2.5 mA constant current anemometer so that a temperature profile could be obtained. The hot wire was then connected to the 1:1 bridge of an TSI IFA-100. The square wave frequency response of the hot wire, in still air at ambient pressure, was 200 kHz. The stagnation temperature in the jet was 427K. From these measurements, the Reynolds number and Nusselt number calibration curve was calculated and compared to the calibration curve of Weltmann and Kuhns [32] as illustrated in Figures 30 and 31. Fair agreement was now found between the current and previously obtained data.

The temperature recovery ratio was also calculated and plotted versus the Knudsen number, Figure 32, along with data from Weltmann and Kuhns [32]. There is a large offset in the temperature recovery ratio which has not yet been explained but is currently being investigated.

Hot-Wire Measurements on Blunt Cones

A 22.25-inch-long blunt cone with a 7-deg. half-angle was also tested in the Mach-6 tunnel. This cone has a 5.5-inch base diameter and a precision nosetip with a 0.020-in. radius. The cone was machined in three different pieces and the pieces were assembled

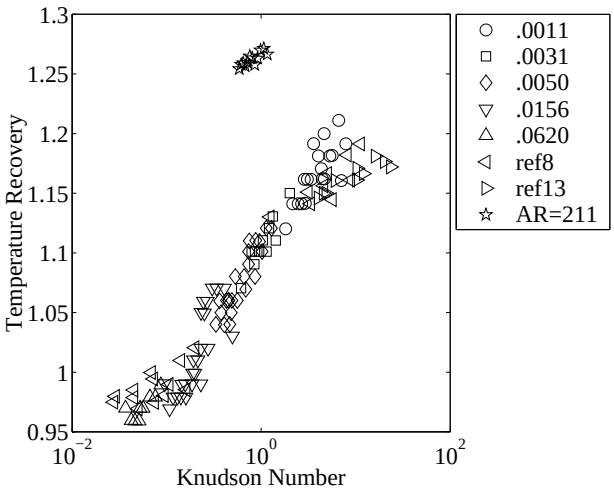

Figure 32: Knudson number vs. Temperature Recovery Ratio

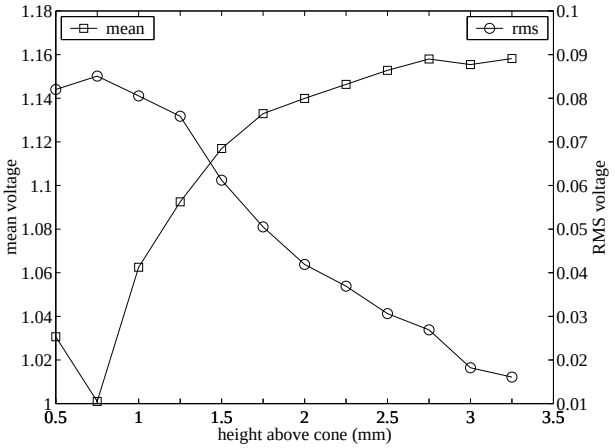

Figure 33: Boundary-layer profile of a 7-deg. blunt cone at zero angle of attack

using socket-head cap screws. The screws are placed in the center shaft of the cone and threaded into the cone pieces to draw the sections together in a tight fit. The maximum step between the joints was 0.0005 inches.

The cone was placed in the test section of the tunnel at zero angle of attack. Hot wire A, which has a cold resistance of 9.05 ohms and an aspect ratio of approximately 115, was placed approximately 14.25 inches axially downstream of the nose. This aspect ratio is somewhat lower than desired and end-loss corrections may be necessary in the future. The overheat ratio (based on resistances) was set to 1.93, so the wire is mostly sensitive to massflow fluctuations. The square wave frequency response using a 1:1 bridge on a TSI IFA-100 was 272 kHz, as measured in still air at ambient pressure. Each run consisted of one height above the wall and all measurements were taken for the same time-step (0.40-0.45s) during the run. The initial driver pressure for each run was set to 125 psia, the driver temperature was $160°C$, and the dewpoint was $-22°C$.

The boundary layer profile for this case is shown in Figure 33. It appears from this figure that the edge of the boundary layer is reached around 2.75 mm above the cone wall. The rms voltage peak occurs closer to the wall than expected. These measurements were compared with computational data (Figure 34) and the experimental boundary layer is found to be thicker, possibly due to difficulties in measuring the height of the hot wire above the wall. A telemicroscope for measuring this height in-situ only recently became operational, since it required a special lens assembly to correct for the distortions caused by the curved nozzle window. Tyler Robarge duplicated the experimental conditions for this comparison using the STABL code, which combines an axisymmetric Navier-Stokes solver with a PSE stability code [33, 34]. The computation predicts the velocity will reach 99% of the freestream value at 1.8 mm above the cone wall.

Variations in the amplitudes of the uncalibrated hot-wire fluctuations are shown as a function of the height above the cone in the power spectra of Figure 35. A close-up of the apparent instability waves is illustrated in Figure 36. The instability wave occurs near 235-240 kHz and the amplitude increases with distance from the wall until reaching its peak at approximately 3.0 mm, near the edge of the boundary layer, as expected. No instability is apparent until the hot wire reaches a height, y, of 1.0 mm above the wall.

The measured frequency at which the instability occurs is higher than expected if comparing to the approximation $f = u_e/2\delta$, which is 160 kHz for this case. A Mach number of 6 and a stagnation temperature of 433 K are used to calculate the edge velocity, u_e, and a boundary layer thickness, δ, of 2.75 mm was used. This frequency is about two-thirds of the frequency obtained from the spectra. However, Tyler Robarge computed near the experimental conditions again using the STABL code and calculated the amplification rate for the second mode instability. The computations were carried out for Mach 5.8, 125 psia stagnation pressure, zero angle of attack, at an arc length of 0.3625 m. This wave, shown in Figure 37, is most amplified at a frequency of approximately 232kHz. The agreement with the experimental data is encouraging. Calculations to find the amplitude vs. frequency plot using the e**N method are underway so that a more accurate comparison can be made between the com-

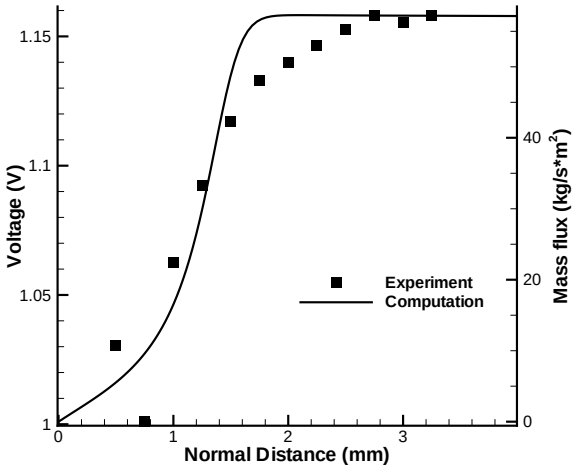

Figure 34: Boundary-layer profile comparison between experiments and computations of a 7-deg. blunt cone at zero angle of attack and 125 psia - experimental data points are represented by the squares and the computational data by the curve-fit

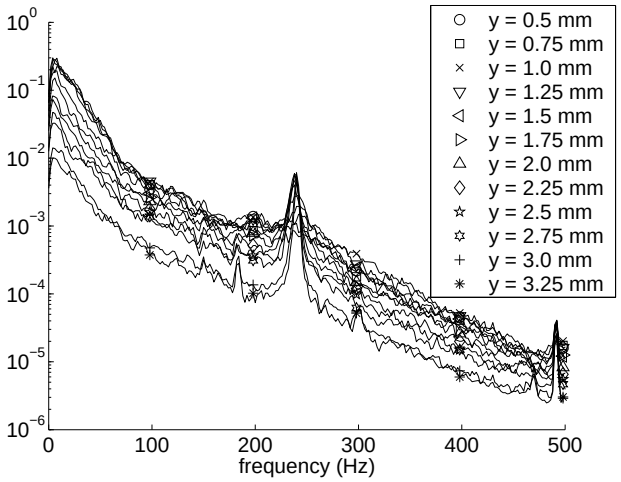

Figure 35: Power Spectra for a 7-deg. blunt cone at zero angle of attack

putations and experiments.

TSP Tests with Digital SLR Camera and Plastic Insulator

Temperature sensitive paint images of a 7-deg. sharp cone with three-inch base diameter at zero angle-of-attack have been taken to test the use of a commercial digital SLR camera and plastic insulator layer in making TSP measurements. A 13.5 Megapixel Kodak DCS Pro 14n camera with a Nikon Zoom AF Nikkor 28-200 mm f/3.5-5.6G ED-IF lens was used. The camera was controlled from a PC with Kodak Camera Manager via an IEEE 1394 connection. Images were captured at 6 MP for these preliminary tests. Camera Manager saved the images directly to the hard drive on the computer. White PVC Type 1 adhesive-backed plastic film was used as an insulator underneath the thermal paint. The insulator layer was 0.0045 inches thick, similar to the DuPont ChromaClear paint insulator layer used previously [11]. The plastic was found to be smoother, more uniform, and easier to apply than the painted insulator, except for a few small bubbles that occurred as the plastic was rolled onto the cone. It should be possible to apply the plastic without these bubbles after some experimentation. The TSP layer consisted of Ru(bpy) luminophore in DuPont ChromaClear paint and was sprayed on as before [35]. An ISSI LM4 blue

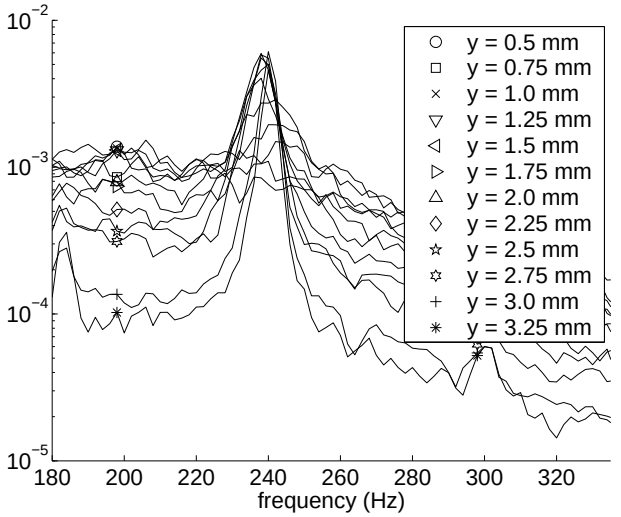

Figure 36: Closeup of the Power Spectra for a 7-deg. blunt cone at zero angle of attack

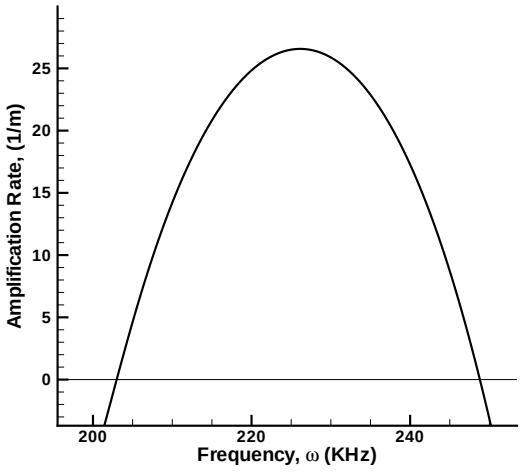

Figure 37: Computed Amplification rate for 7-deg. blunt cone

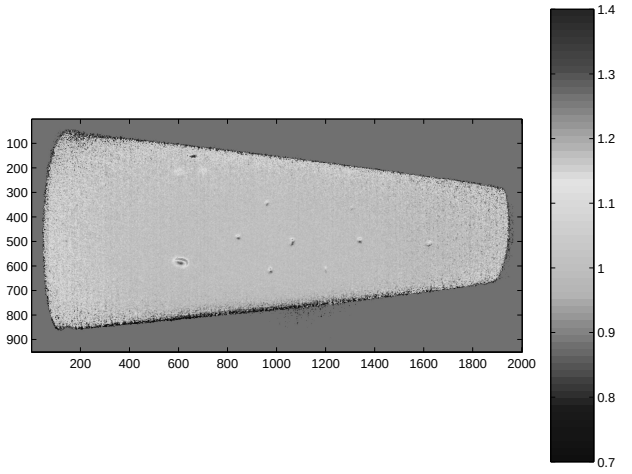

Figure 38: TSP Image of 7-deg Sharp Cone at Zero Angle-of-Attack Taken with Commercial SLR

(464 nm) light-emitting-diode array was used to illuminate the surface of the cone. An Oriel Corp. 600 nm high-pass filter was placed over the lens to allow only emitted radiation into the lens.

Figure 38 shows an image of the cone at $Re_\infty = 3 \times 10^6$/ft in the Mach 6 Ludwieg tube. The image shows mostly laminar flow over the 12.217-in long cone, as expected [11]. The dots at the rear of the cone may indicate the early stages of transition or could just be noise. A few bubbles in the plastic layer can be seen in the image, as can some fiducial marks placed on the cone to aid in focusing the camera, although both of these are more evident in the original color image. Focusing was done manually, since autofocus does not work well through the test section window. The image has more noise than previous images taken with a scientific-grade CCD camera. The imager in the Kodak is not cooled, resulting in more thermal noise.

The Kodak camera is capable of producing pictures with 12-bit resolution per color channel (RGB). However, only 8-bit resolution has been attained so far. This could be a processing issue and will be addressed. The digital SLR should prove a useful tool for qualitative TSP measurements.

The plastic insulator performed well in these preliminary tests. It rolls onto the cone fairly easily and takes the ChromaClear paint without fouling. Our scientific-grade, 12-bit CCD camera was recently repaired, and will be used to better determine the thermal performance of the plastic film as an insulator.

Summary

Purdue University continues to develop the 9.5-inch Mach-6 Boeing/AFOSR Mach-6 Quiet Tunnel. So far, quiet flow has only been achieved at 8 psia stagnation pressure, probably because of a separation bubble found in computations on the bleed lip. Preliminary measurements in the contraction inlet find massflow fluctuations of 0.13-0.19%. These are comparable to the 0.2% velocity fluctuations reported by Beckwith in the Langley Mach 3.5 quiet tunnel, suggesting that while the inlet flow is imperfect it is probably not tripping the boundary layer. Measurements of the effects of downstream perturbations also continue. These continue to show that separations are easily induced in a laminar nozzle-wall boundary layer, as expected, but show no evidence that the 8 psia transition is caused by downstream noise. The Case-8 bleed-slot throat insert attempted to solve the apparent separation problem by increasing the suction massflow to near 50%. It failed, apparently because the increased massflow required for a sonic bleed throat was beyond the capabilities of the suction system.

The tunnel is being modified to run at higher pressures, with presumably conventional noise, to study transition and the transition mechanisms for blunt cones at angle of attack. A porthole window was recently delivered, enabling temperature-sensitive paint measurements to 6×10^6 per foot. Earlier measurements by Boudreau et al. suggest this is sufficient to study frustum transition induced by distributed nosetip roughness.

Hot-wire calibrations are also progressing. Corrections to the throat geometry of the calibration nozzle have eliminated high fluctuation levels in the core and

enabled Nusselt-Reynolds calibrations in fair agreement with the literature. The recovery factors that have been obtained are still far above those in the literature, for unknown reasons. Preliminary hot-wire measurements on a 0.5-mm nose-radius blunt cone find apparent second-mode instability waves at about 235 kHz, in good agreement with linear-instability computations. However, the experimental boundary-layer profile appears to be much thinner than in the computation.

Acknowledgements

The research is funded by AFOSR under grant F49620-03-1-0030, and by Sandia National Laboratory under contract 80377. Frank Chen and Steve Wilkinson from NASA Langley continued to provide occasional assistance in making the best possible use of information available from the earlier NASA Langley quiet-tunnel development effort. Mr. Gerald Hahn of the AAE machine shop noticed the problems with the throat of the hot-wire calibration jet, and designed and machined the modification to provide smooth flow surfaces.

REFERENCES

[1] Steven P. Schneider. Hypersonic laminar-turbulent transition on circular cones and scramjet forebodies. *Progress in Aerospace Sciences*, 40(1-2):1–50, 2004.

[2] I.E. Beckwith and C.G. Miller III. Aerothermodynamics and transition in high-speed wind tunnels at NASA Langley. *Annual Review of Fluid Mechanics*, 22:419–439, 1990.

[3] Steven P. Schneider. Effects of high-speed tunnel noise on laminar-turbulent transition. *Journal of Spacecraft and Rockets*, 38(3):323–333, May–June 2001.

[4] Steven P. Schneider. Flight data for boundary-layer transition at hypersonic and supersonic speeds. *Journal of Spacecraft and Rockets*, 36(1):8–20, 1999.

[5] S. P. Wilkinson, S. G. Anders, and F.-J. Chen. Status of Langley quiet flow facility developments. Paper 94-2498, AIAA, June 1994.

[6] I. Beckwith, T. Creel, F. Chen, and J. Kendall. Freestream noise and transition measurements on a cone in a Mach-3.5 pilot low-disturbance tunnel. Technical Paper 2180, NASA, September 1983.

[7] Alan E. Blanchard, Jason T. Lachowicz, and Stephen P. Wilkinson. NASA Langley Mach 6 quiet wind-tunnel performance. *AIAA Journal*, 35(1):23–28, January 1997.

[8] S. P. Schneider and C. E. Haven. Quiet-flow Ludwieg tube for high-speed transition research. *AIAA Journal*, 33(4):688–693, April 1995.

[9] Steven P. Schneider. Design of a Mach-6 quiet-flow wind-tunnel nozzle using the e**N method for transition estimation. Paper 98-0547, AIAA, January 1998.

[10] Steven P. Schneider, Shin Matsumura, Shann Rufer, Craig Skoch, and Erick Swanson. Progress in the operation of the Boeing/AFOSR Mach-6 quiet tunnel. Paper 2002-3033, AIAA, June 2002.

[11] Steven P. Schneider, Shin Matsumura, Shann Rufer, Craig Skoch, and Erick Swanson. Hypersonic stability and transition experiments on blunt cones and a generic scramjet forebody. Paper 2003-1130, AIAA, January 2003.

[12] Steven P. Schneider, Craig Skoch, Shann Rufer, and Erick Swanson. Hypersonic transition research in the Boeing/AFOSR Mach-6 quiet tunnel. Paper 2003-3450, AIAA, June 2003.

[13] Steven P. Schneider, Craig Skoch, Shann Rufer, Erick Swanson, and Matt Borg. Bypass transition on the nozzle wall of the Boeing/AFOSR Mach-6 quiet tunnel. Paper 2004-0250, AIAA, January 2004.

[14] Steven P. Schneider, Shann Rufer, Craig Skoch, Erick Swanson, and Matthew P. Borg. Instability and transition in the Mach-6 quiet tunnel. Paper 2004-2247, AIAA, June 2004.

[15] Ezgi S. Taskinoglu, Doyle D. Knight, and Steven P. Schneider. A numerical analysis for the bleed slot design of the Purdue Mach-6 wind tunnel. Paper 2005-0901, AIAA, January 2005.

[16] D. Fisher, K.H. Horstmann, and H. Riedel. Flight test measurement techniques for laminar flow. AGARDograph 300, NATO Research and Technology Organization, 2003.

[17] Steven P. Schneider. Design and fabrication of a 9-inch Mach-6 quiet-flow Ludwieg tube. Paper 98-2511, AIAA, June 1998.

[18] I.E. Beckwith, F.J. Chen, and T.R. Creel. Design requirements for the NASA Langley supersonic low-disturbance wind tunnel. Paper 86-0763, AIAA, 1986.

[19] Daniel C. Reda. Correlation of nosetip boundary-layer transition data measured in ballistics-range experiments. *AIAA Journal*, 19(3):329–339, March 1981.

[20] R. G. Batt and H.H. Legner. A review of roughness-induced nosetip transition. *AIAA Journal*, 21(1):7–22, January 1983.

[21] A.H. Boudreau. Artificially induced boundary-layer transition on blunt-slender cones using distributed roughness and spherical-type tripping devices at hypersonic speeds. Technical Report AEDC-TR-77-120, Arnold Engineering Development Center, February 1978.

[22] A.H. Boudreau. Artificially induced boundary-layer transition on blunt-slender cones at hypersonic speeds. *Journal of Spacecraft and Rockets*, 16(4):245–251, July-August 1979.

[23] A.H. Boudreau. Correlation of artificially induced boundary-layer transition data at hypersonic speeds. *Journal of Spacecraft and Rockets*, 18(2):152–156, March-April 1981.

[24] S.W. Kwon and Steven P. Schneider. Stress analysis for the window of the Purdue Mach-6 quiet-flow Ludwieg tube. Paper 2002-0309, AIAA, January 2002.

[25] M.R. Snoey and J.D. Stachiw. Windows and transparent hulls for man in hydrospace. In *A critical look at marine technology, transactions of the 4th annual MTS conference and exhibit*, pages 419–463. Marine Technology Society, July 1968. Conference was held in Washington, DC. OCLC number 35224051.

[26] J.D. Stachiw, O.M. Dunn, and K.O. Gray. Windows for external or internal hydrostatic pressure vessels. Part II. Flat acrylic windows under short-term pressure application. Technical Report TR-R-527, Naval Civil Engineering Laboratory, May 1967. DTIC citation AD652343.

[27] George Xu. Structural analysis of the Purdue University Mach-6 quiet flow nozzle large window. Tri-Models, Inc., Huntington Beach, CA. Revision C, 21 Dec. 2004. Tri-Models model number 4325-001. Report on file at Purdue Aerospace Sciences Lab.

[28] Steven P. Schneider and Craig Skoch. Mean flow and noise measurements in the Purdue Mach-6 quiet-flow Ludwieg tube. Paper 2001-2778, AIAA, June 2001.

[29] Craig Skoch. Leak testing. Informal lab report in draft form, dated 5 April 2004. 6 pages.

[30] Phillip M. Schneider. Design and construction of a Mach 6 hot wire calibration jet. Purdue University, School of Aeronautics and Astronautics. A 30 page laboratory report, plus extensive appendices, December 1998.

[31] Phillip M. Schneider. Flow measurements in a Mach 4 axisymmetric jet. Purdue University, School of Aeronautics and Astronautics. A 29 page laboratory report with 11 figures, May 1999.

[32] Ruth N. Weltmann and Perry W. Kuhns. Heat transfer to cylinders in crossflow in hypersonic rarefied gas streams. Technical Note TN-D-267, NASA, March 1960.

[33] Tyler Robarge and Steven P. Schneider. Mean flows and instabilities on blunt cones at hypersonic speeds. Paper 2005-XXXX, AIAA, June 2005. Submitted to the Toronto Fluid Dynamics Meeting.

[34] Heath B. Johnson and Graham V. Candler. STABL: A method for analyzing hypersonic boundary layer stability. Paper 2005-XXXX, AIAA, June 2005. Submitted for Toronto Fluid Dynamics Meeting.

[35] Erick Swanson. Mean flow measurements and cone flow visualization at Mach 6. Master's thesis, School of Aeronautics and Astronautics, Purdue University, December 2002.